RESEARCH ARTICLE

Enhancing the catalytic efficiency of *Fusarium oxysporum* deoxynivalenol detoxifying enzyme through computational design and targeted mutation

Nan Cui*

Luoyang Vocational College of Culture and Tourism, Luoyang, Henan, China.

Received: March 26, 2026; **accepted:** July 11, 2026.

Deoxynivalenol (DON, vomitoxin) is one of the most widely contaminated fungal toxins in grains, posing a serious threat to food safety and human health. The existing natural DON detoxifying enzymes have bottleneck problems such as low catalytic efficiency, poor environmental adaptability, and insufficient substrate affinity. This study constructed a three-dimensional structural model of DON epoxyhydrolase based on multi-scale computational biology methods. By combining free energy decomposition, transition state analysis, and saturation mutation calculation, four key regulatory sites were screened, and site directed mutagenesis technology was used to complete the directed modification of enzyme molecules. The study established a strategy for reconstructing the microenvironment of catalytic pockets, a mechanism for stabilizing transition states, and an optimization method for hydrogen bonding networks, achieving a joint optimization of enzyme affinity for substrates, catalytic conversion efficiency, and environmental stability. The results showed that the optimal four-site combination mutant M4 (Ser135Ala/Val218Leu/Gln180His/Thr245Ser) achieved a catalytic efficiency (kcat/Km) 5.51 times that of the wild type in both test systems, a 61.9% decrease in Michaelis constant (Km) compared to the wild type, an increase in the optimal temperature from 35℃ to 45℃, and a widening of the pH adaptation range of 4.5 - 7.0. In the 10 μg/mL DON substrate system, the degradation rate of the mutant after 2 hours of reaction was close to 100%, which was 137% higher than that of the wild type. In actual wheat contaminated substrates, the degradation rate of 5 mg/kg DON reached 92% with an enzyme dosage of 20 U/g, and the enzyme activity retention rate still reached 78% after 5 cycles of use. Under extreme pH and high temperature conditions, the enzyme activity retention rate of the mutant was more than three times higher than that of the wild type, while maintaining catalytic specificity for DON epoxide ring hydrolysis without the generation of by-products. This study provided a scalable computational design and experimental verification technology path for the efficient targeted modification of fungal toxin detoxifying enzymes. The highly active mutant obtained had broad application prospects in the field of grain fungal toxin biological detoxification, suitable for multiple scenarios such as grain storage, feed processing, and food deep processing.

Keywords: deoxynivalenol; detoxifying enzyme; site directed mutation; catalytic efficiency.

***Corresponding author:** Nan Cui, Luoyang Vocational College of Culture and Tourism, Luoyang, Henan 471000, China. Email: 15672781759@163.com.

Introduction

With the upgrading of global food security demand, deoxynivalenol (DON) contamination caused by *Fusarium* infection poses a serious threat to grain quality and food safety. Enzymatic biological detoxification has become the mainstream direction due to its strong specificity and pollution-free advantages. The current mainstream enzyme molecular computational

design system usually consists of multiple modules that work together including structural modeling, molecular docking, dynamic simulation, free energy calculation, and mutation site screening. This system needs to simultaneously face the dynamic flexibility of protein structure, substrate binding specificity, energy barrier limitations of catalytic reactions, and multidimensional effects of environmental factors. In practical research, the modification process of enzyme molecules always revolves around a closed-loop process of structural analysis, mechanism analysis, site design, and performance verification, and achieves full dimensional regulation from the atomic level to the molecular level through multi-scale computational methods.

Adegok *et al*. optimized microbial detoxifying enzymes through site directed mutagenesis, confirming the core value of this technology in improving performance, but also highlighting the difficulty of precise screening of key sites [1]. Further, scientists used computational biology to analyze the catalytic structure and substrate interaction mechanism of DON detoxifying enzymes from different sources, laying the foundation for rational design [2]. Pedroni *et al*. constructed a "computational simulation prediction *in vitro* experimental verification" system and successfully applied it to the development of *Fusarium* acid detoxifying enzyme, providing a methodological framework [3]. Luo *et al*. analyzed the mechanism of DON accumulation and detoxification from the perspective of wheat *Fusarium graminearum* interaction and clarified the technical application requirements [4]. Sun *et al*. reviewed the bottlenecks of low catalytic efficiency and poor adaptability of natural DON detoxifying enzymes and pointed out that rational design of structural biology was the key breakthrough [5]. Della Gala compared enzymatic strategies and confirmed the advantages of cyclooxygenase in DON detoxification but pointed out stability and cost issues [6]. Zhou *et al*. optimized the maize zearalenone converting enzyme ZPH13 through site directed mutagenesis and confirmed the key regulatory role of non-catalytic site modification [7]. Wang *et al*. developed a synthetic microbial community system, highlighting the core position of high-performance detoxifying enzymes in the full chain prevention and control of fungal toxins [8]. Iñiguez-Luna *et al*. elucidated the application of molecular docking in target screening and validated the efficiency of computational simulations [9]. Yang *et al*. analyzed the regulation of catalytic efficiency by the evolution of the TRI101/201 family enzyme loop region, providing structural basis for the modification of epoxy hydrolases [10]. Dumbai *et al*. analyzed the resistance mechanism of *Fusarium* to fungicides, emphasizing the irreplaceability of enzymatic detoxification [11]. Varadharajan *et al*. reviewed the application of multi-omics techniques in anti-stress target mining, providing a method for verifying the effectiveness of enzyme modification [12]. Chtioui *et al*. developed source control for phenolic substances, but there were shortcomings such as unstable field effects and inability to treat contaminated grains [13]. Tundo *et al*. analyzed the effects of plant derived xylanase inhibitors and expanded enzymatic resources [14]. Mateo *et al*. summarized the application of artificial intelligence in toxin prevention and control, providing ideas for subsequent intelligent optimization [15]. Schueller *et al*. developed a fungal genome mining tool to assist in the discovery of novel detoxifying enzymes [16]. Narula *et al*. analyzed fungal host interactions through proteomics, providing a biological basis for the adaptation of detoxification enzyme application scenarios [17]. Younas *et al*. summarized the biological stress resistance technology of fruits and vegetables, which could be extended to grain control [18]. Although existing research has made significant progress in the modification of DON detoxifying enzymes, there are still major limitations that restrict their industrial applications. Most studies only focus on optimizing single catalytic performance, lacking a multi-objective collaborative design system that can simultaneously improve substrate affinity, catalytic efficiency, stability, and substrate compatibility [19-22]. Further, there is

insufficient analysis of the atomic mechanism of DON epoxidase catalyzed transition state stabilization, making it difficult to achieve precise modification at the atomic level. Furthermore, a complete multi-scale computational design system that integrates homology modeling, full atomic dynamics simulation, free energy decomposition, and quantum mechanics/ molecular mechanics (QM/MM) combined transition state analysis has not yet been formed, resulting in insufficient ability for precise screening and efficient verification of key sites [23-26].

This study proposed a targeted modification strategy for DON detoxifying enzymes based on multi-scale computational design and site directed mutagenesis to break through the catalytic efficiency bottleneck of natural detoxifying enzymes. The study constructed a high-precision three-dimensional structural model of wild-type DON epoxide hydrolase based on homology modeling and molecular dynamics simulation, accurately screened key sites regulating substrate binding and catalytic efficiency by combining molecular mechanics Poisson-Boltzmann surface area (MM-PBSA) free energy decomposition, saturation mutation calculation, and QM/MM transition state energy barrier analysis, and completed the performance validation and optimization of mutants through site directed mutagenesis, protein expression purification, and enzymatic characterization. This study achieved precise modification of enzyme molecules at the atomic level through the organic combination of catalytic pocket microenvironment reconstruction, hydrogen bond network optimization, and transition state stabilization mechanism, which provided not only a scalable technical path for the efficient modification of fungal toxin detoxifying enzymes and other industrial enzymes, but also core materials and technical support for the green biological detoxification of grain fungal toxins.

Materials and methods

Homology modeling and molecular dynamics simulation

All computational calculations were performed on a high-performance computing server equipped with Intel Xeon Gold 6330 CPU (Intel Corp., Santa Clara, CA, USA), NVIDIA A100 GPU (NVIDIA Corp., Santa Clara, CA, USA) with 80 GB video memory, and Ubuntu Server 22.04 operating system. The amino acid sequence of wild-type *Fusarium oxysporum* DON epoxide hydrolase was obtained from the National Center for Biotechnology Information (NCBI) GenBank (https://www.ncbi.nlm.nih.gov/genbank/) with the accession number of XP_018247632.1. Homology modeling was performed using the SWISS-MODEL (https://swissmodel.expasy.org/) with the crystal structure of *Fusarium graminearum* epoxide hydrolase (PDB ID: 6L2X) as the template, which shared 78% sequence identity with the target protein. The quality of the constructed model was evaluated by using PROCHECK (https://github.com/RomanLas/PROCHECK) and Verify3D (https://www.doe-mbi.ucla.edu/verify3d/). Molecular docking was performed using AutoDock Vina 1.2.3 (https://vina.scripps.edu/). The three-dimensional structure of DON substrate was obtained from the PubChem database (https://pubchem.ncbi.nlm.nih.gov/) with the CID of 40024. The docking grid box was centered on the catalytic triad Asp129-His242-Glu156 with dimensions of 20 Å × 20 Å × 20 Å. The optimal docking conformation was selected based on the lowest binding energy and correct orientation of the epoxy ring towards the catalytic triad. All molecular dynamics simulations were performed using Amber 20 (https://ambermd.org/). The protein force field used was AMBER ff14SB, the substrate small molecule force field was GAFF2, and the water molecule model was TIP3P. The system was constructed using a cubic water box with a distance of 10 Å between the protein and the box boundary. Na^+ and Cl^- ions were added to neutralize the system and adjust the ionic strength to 0.15 mol/L. Energy optimization was performed in two steps including 5,000 steps of steepest descent followed by 5,000 steps of conjugate gradient with constrained protein,

then another 5,000 steps of steepest descent and 5,000 steps of conjugate gradient without constraints. The simulation was performed under NPT ensemble at 300 K and 1 bar using Langevin dynamics for temperature control and Parrinello-Rahman method for pressure control. The integral step size was 2 fs, and the trajectory was sampled every 10 ps for a total simulation duration of 100 ns. The trajectory analysis was performed using cpptraj module in Amber 20.

Free energy calculation and key residue screening

Binding free energy calculation was performed using the MM-PBSA module in Amber 20 software. A total of 1,000 frames were extracted from the last 20 ns of the equilibrium trajectory for calculation. The ionic strength was set to 0.15 mol/L, while the internal dielectric constant of the protein was 1, and the solvent dielectric constant was 80. Single residue binding free energy decomposition was performed for all residues within 5 Å of the catalytic pocket to screen non-catalytic residues with significant contributions to substrate binding (ΔG_bind, res < -1 kcal/mol).

Mutation design and optimization

Saturation mutation calculation and Rosetta design optimization were performed using Rosetta 3.12 (https://www.rosettacommons.org/). For each screened key residue, all 19 possible amino acid mutations were calculated, and the optimal mutation type was selected based on the change in binding free energy (ΔΔG) and structural stability. To verify the independent contribution and synergistic effect of different mutation modules, a systematic ablation experiment scheme was designed with single-point mutant M1 (Ser135Ala), M2 (Val218Leu), double-point mutant M3 (Gln180His/Thr245Ser), four-site combination mutant M4 (Ser135Ala/Val218Leu/Gln180His/Thr245Ser). Wild-type (WT) enzyme was used as the control group.

Transition state analysis

Density functional theory (DFT) combined with QM/MM method was used to construct the reaction pathway of DON epoxide ring hydrolysis catalyzed by wild-type and mutant enzymes. All quantum chemistry calculations were performed using Gaussian 16 (https://gaussian.com/). The catalytic triad and substrate molecule were included in the QM region, which was treated at the B3LYP/6-31G (d, p) level of theory. The rest of the system was included in the MM region, which was treated with the AMBER ff14SB force field. The transition state structure was located by Berny optimization and verified by frequency calculation (only one imaginary frequency). The activation energy barrier of the reaction was calculated as the difference between the free energy of the transition state and the ground state.

Site directed mutagenesis and recombinant plasmid construction

The wild-type DON epoxide hydrolase coding gene was amplified from the genomic DNA of *Fusarium oxysporum* strain CGMCC 3.17624, which was purchased from the China General Microbiological Culture Collection Center (CGMCC) (Beijing, China). Genomic DNA extraction was performed using the Fungal Genomic DNA Extraction Kit (Tiangen Biotech Co., Ltd., Beijing, China) according to the manufacturer's instructions. Site directed mutagenesis primers were designed based on four mutation sites of Ser135Ala, Val218Leu, Thr245Ser, Gln180His using Primer Premier 5.0 software (https://www.premierbiosoft.com/) (Table 1). The gene amplification of single point mutation and combination mutation was completed using overlapping extension polymerase chain reaction (PCR) method. PCR reactions were performed using a Veriti 96-Well Thermal Cycler (Applied Biosystems, Foster City, CA, USA). The PCR reaction system was 50 μL including 25 μL of 2× Phanta Max Master Mix, 2 μL each of upstream and downstream primers, 1 μL of template DNA, and 20 μL of enzyme free water. The PCR program was 95℃ for 3 minutes followed by 30 cycles of 95℃ for 15 seconds, 58℃ for 15 seconds, 72℃ for 1 kb/min, and a final 72℃ for 5 minutes. After the PCR product was verified by 1% agarose gel electrophoresis,

Table 1. Primer sequences for site directed mutation.

Mutation site	Primer sequence (5' - 3')	Annealing temperature (°C)
Ser135Ala	GCT GGT TCT GCG GCT ATC GGT ACC	58
	GGT ACC GAT AGC CGC AGA ACC AGC	58
Val218Leu	CAA GTT CAT TTG CTG GAC CTG AAG	58
	CTT CAG GTC CAG CAA ATG AAC TTG	58
Gln180His	GAT GAC AAC CAT TTC AAC GAG TGG	57
	CCA CTC GTT GAA ATG GTT GTC ATC	57
Thr245Ser	CAT TTC CGG TTC TTC CGG TAC GAT	58
	ATC GTA CCG GAA GAA CCG GAA ATG	58

the target fragment was purified using Omega Bio-tek Gel Extraction Kit (Omega Bio-tek, Norcross, GA, USA). The purified fragment and pET-28a(+) expression vector (Novagen, Madison, WI, USA) were double digested with restriction endonucleases BamH I and Xho I (New England Biolabs, NEB, Ipswich, MA, USA) at 37°C for 2 hours, then ligated using T4 DNA ligase (NEB, Ipswich, MA, USA) at 16°C overnight. The ligation product was transformed into *Escherichia coli* DH5α competent cells (Takara Bio Inc., Dalian, Liaoning, China) by heat shock at 42°C for 90 seconds and plated on LB solid medium containing 50 μg/mL Kanamycin. After overnight culture at 37°C, single colonies were picked for PCR verification and Sanger sequencing (Sangon Biotech Co., Ltd., Shanghai, China). Positive clones were inoculated into LB liquid medium, and plasmids were extracted using Omega Bio-tek Plasmid Mini Kit (Omega Bio-tek, Norcross, GA, USA). The verified recombinant plasmids were transformed into *Escherichia coli* BL21(DE3) competent cells (Takara Bio Inc., Dalian, China) for subsequent protein expression.

Induced expression and purification of proteins

A single colony of *Escherichia coli* BL21(DE3) containing recombinant plasmids was inoculated into LB liquid medium containing 50 μg/mL Kanamycin and shaken at 37℃ and 220 rpm until the OD_{600} reaching 0.6 - 0.8. Subsequently, isopropyl-β-D-thiogalactoside (IPTG) was added to a final concentration of 0.5 mM and induced for expression at 16°C and 180 rpm for 16 hours. After induction, the bacterial cells were collected by centrifugation at 4°C and 8,000 rpm for 10 minutes, and the precipitate was resuspended in binding buffer containing 20 mM Tris-HCl, 500 mM NaCl, 20 mM imidazole, pH 8.0 and sonicated under ice bath conditions using JY92-IIN ultrasonic disruptor (Ningbo Xinzhi Biotechnology Co., Ltd., Ningbo, Zhejiang, China) with 300 W of power, 3 s of ultrasound, 5 s of interval, a total of 99 cycles. The crushing solution was centrifuged at 4℃ and 12,000 rpm for 30 minutes. The supernatant was collected and filtered through a 0.22 μm membrane before being loaded onto a pre-equilibrated HisTrap HP Ni-NTA affinity chromatography column (GE Healthcare, Uppsala, Sweden) connected to an ÄKTA Pure 25 protein purification system (GE Healthcare, Uppsala, Sweden). Gradient elution was performed using elution buffer solutions containing 20 mM, 50 mM, and 250 mM imidazole, respectively. The elution peaks of the target protein were collected, and their purity was verified by 12% SDS-PAGE. The protein components were dialyzed with 20 mM Tris-HCl and 150 mM NaCl in dialysis buffer at pH 8.0 and 4℃ overnight to remove imidazole and high concentration salts. After dialysis, the protein was concentrated using MWCO 10 kDa Amicon Ultra-15 ultrafiltration tube (Millipore, Billerica, MA, USA), and the concentration was determined using a BCA protein quantification kit (Thermo Fisher Scientific, Waltham, MA, USA). After packaging, the protein was stored at -80℃ for future use.

Characterization of enzymatic properties and degradation performance

(1) Enzyme activity assay

The standard enzyme activity assay system contained 10 μg/mL DON, 50 mM citrate buffer (pH 5.5), and an appropriate amount of enzyme solution in a total volume of 1 mL. The reaction mixture was incubated at 37℃ for 30 minutes, then terminated by adding 1 mL of methanol. The concentration of residual DON was determined by high-performance liquid chromatography (HPLC). One enzyme activity unit (U) was defined as the amount of enzyme required to degrade 1 μg of DON per minute under the above conditions.

(2) Determination of pH and temperature adaptability

To determine the optimal pH of the enzyme, the enzyme activity was measured at 37°C in buffer solutions with pH values ranging from 3.0 to 10.0 (citrate buffer for pH 3.0 - 6.0, phosphate buffer for pH 6.0 - 8.0, and Tris-HCl buffer for pH 8.0 - 10.0). To determine the optimal temperature, the enzyme activity was measured at temperatures ranging from 20°C to 70°C at the optimal pH. The pH stability was determined by pre-incubating the enzyme in buffer solutions with different pH values at 4°C for 24 hours, then measuring the residual enzyme activity under standard conditions. The thermal stability was determined by pre-incubating the enzyme at different temperatures for 1 hour, then measuring the residual enzyme activity under standard conditions. The enzyme activity under optimal conditions was defined as 100%.

(3) DON degradation performance assay in liquid phase system

The DON degradation performance of enzymes was evaluated under different substrate concentrations of 10 - 200 μg/mL, reaction temperatures of 30 - 50℃, pH values of 4.0 - 8.0, and reaction times of 0.5 - 6 hours. The degradation rate of DON was calculated as follows.

$$\text{Degradation rate (\%)} = (C_0 - C_t)/C_0 \times 100\%$$

where C_0 was the initial concentration of DON. C_t was the concentration of DON at time t. The degradation products were qualitatively analyzed by TSQ Quantis liquid chromatography-tandem mass spectrometry (LC-MS/MS) (Thermo Fisher Scientific, Waltham, MA, USA). The ion source was an electrospray ion source operated in positive ion mode with a scanning range of m/z 50 - 500.

(4) DON degradation assay in actual grain samples

Naturally DON-contaminated wheat, corn, and barley samples were collected from Luoyang, Henan, China. The initial DON content in the samples was determined by HPLC. The grain samples were ground into powder and passed through a 40-mesh sieve. 10 g of grain powder was mixed with 50 mL of 50 mM citrate buffer (pH 5.5) containing different dosages of enzyme (5, 10, 20 U/g). The mixture was incubated at 37℃ for 2 hours with shaking at 150 rpm. After reaction, the sample was centrifuged at 8,000 rpm for 10 minutes, and the supernatant was collected for DON content determination.

(5) Cyclic stability assay

The enzyme was immobilized on chitosan microspheres according to the method described previously [27, 28]. The immobilized enzyme was used to degrade 10 μg/mL DON solution at 37℃ and pH 5.5 for 2 hours. After each cycle, the immobilized enzyme was recovered by centrifugation, washed three times with buffer, and reused for the next cycle. The enzyme activity retention rate was calculated after 5 cycles of use.

(6) Industrial scaling simulation experiment

Laboratory small-scale experiment was performed in a 1 L reaction system, pilot-scale experiment in a 100 L reaction system, and large-scale production simulation in a 1,000 L reaction system. All experiments were performed under the same conditions with 10 μg/mL DON, 20 U/g enzyme dosage, 37℃, pH 5.5, reaction time 2 hours. The degradation rate of DON was determined after reaction.

Statistical analysis

SPSS 26.0 (IBM, Armonk, NY, USA) was employed in this research for statistical analysis. All experiments were performed in triplicate, and the results were expressed as mean ± standard deviation (SD). One-way analysis of variance (ANOVA) followed by Tukey's multiple comparison test was used to compare the differences between groups. *P* value less than 0.05 was considered statistically significant [29, 30].

Results and discussion

Computational design and mutation screening

The homology modeling results showed that the wild-type *Fusarium oxysporum* DON epoxide hydrolase had a typical (α/β) 8 triose phosphate isomerase (TIM) barrel shaped fold. The catalytic center was located at the C-end opening of the TIM barrel structure and contained the conserved catalytic triad Asp129-His242-Glu156. The hydrophobic cavity area and polar binding area of the catalytic pocket were the core spatial range of substrate binding (Figure 1).

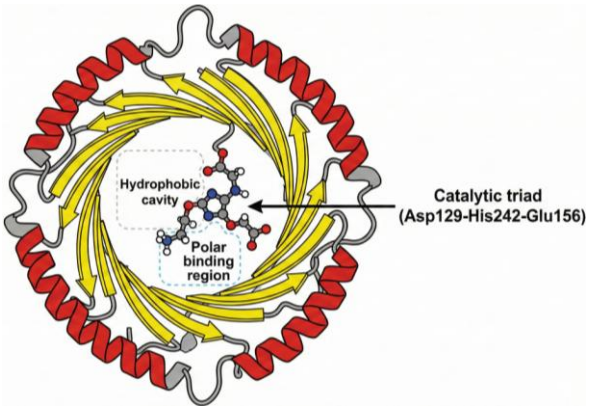

Figure 1. Overall structure of wild-type DON epoxide hydrolase. Red: α helix. Yellow: β fold. Gray: random curls and ring areas. The catalytic triad was labeled with a ball stick model.

Molecular docking results showed that the C12, 13 epoxy ring of DON was oriented towards the catalytic triad, forming bidentate hydrogen bonds with Asp129 at bond lengths of 2.8 Å and 3.1 Å, respectively, and forming electrostatic interactions with His242. The C3 hydroxyl group of the substrate formed stable hydrogen bonds with Tyr216 and Asn178 with bond lengths of 2.9 Å and 3.2 Å, respectively, while the C7 hydroxyl group formed weak hydrogen bonds with Ser135. Meanwhile, hydrophobic residues such as Val218, Leu182, Phe241, *etc*. formed the hydrophobic cavity of the catalytic pocket and interacted with the carbon skeleton of the substrate in a hydrophobic manner (Figure 2).

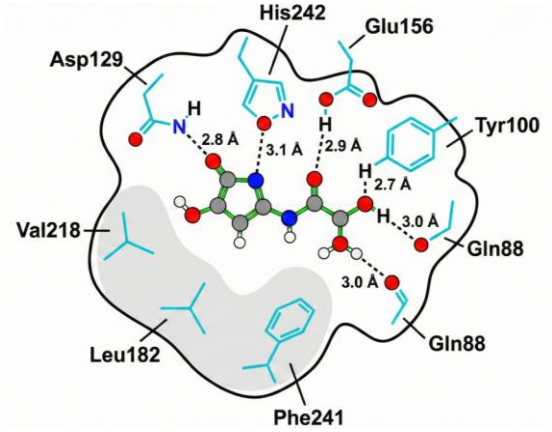

Figure 2. Molecular docking and hydrogen bond coordination network between DON substrate and wild-type enzyme catalytic pocket.

Single residue binding free energy decomposition results showed that four non-catalytic key residues with substrate binding contributions below -1 kcal/mol were identified as Ser135, Val218, Thr245, and Gln180 (Figure 3)

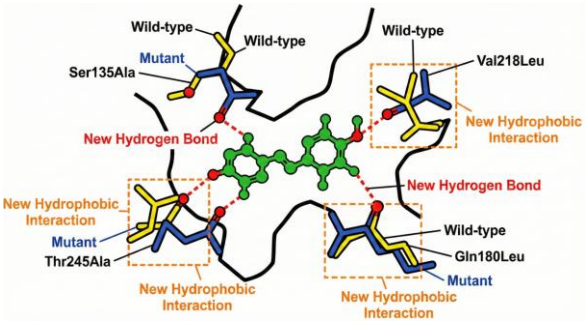

Figure 3. Key residue mutation sites identified based on binding free energy decomposition.

Table 2. Key mutation sites design based on free energy decomposition.

Wild-type residue	mutation site	Residue position	Single residue free energy contribution (kcal/mol)	Mutation type	Change in free energy after mutation ΔΔG (kcal/mol)
Ser	135	Catalytic pocket entrance	-0.82	Ala	-2.36
Val	218	Hydrophobic cavity core	-1.15	Leu	-1.87
Gln	180	Polar binding zone	-0.94	His	-2.15
Thr	245	Catalytic triad surrounding	-0.76	Ser	-1.52

Rosetta design optimization results showed that Ser135Ala mutation enhanced the hydrophobicity of the catalytic pocket. Val218Leu mutation optimized the spatial matching of the hydrophobic cavity. Thr245Ser mutation stabilized the conformation of the catalytic triad. Gln180His mutation added hydrogen bonding interaction with the substrate. All four mutations showed negative ΔG values, indicating that they could improve the binding affinity between enzyme and substrate (Table 2). QM/MM transition state analysis showed that, in the transition state structure of the optimal mutant M4 catalyzing the hydrolysis of DON epoxide ring, the C12, 13 epoxide rings of DON underwent partial ring opening, and the C-O bond length was extended from 1.43 Å in the ground state to 1.98 Å in the transition state (Figure 4).

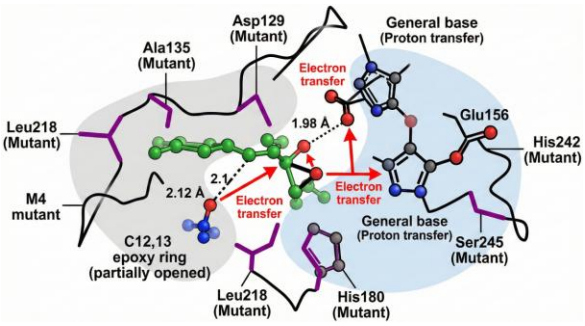

Figure 4. Transition state structure and electron transfer pathway of catalytic reaction of mutant enzyme DON complex.

The oxygen atom of the nucleophilic water molecule formed a partial bond with the C13 atom with a bond length of 2.12 Å. The carboxyl oxygen atom of Asp129 formed a stable hydrogen bond with the O atom of the epoxy ring with a bond length of 2.5 Å. The imidazole ring of His242 functioned as a generalized base and participated in the proton transfer process. The reconstruction effect of four mutant residues on the catalytic pocket microenvironment stabilized the charge distribution of transition states and reduced the activation energy barrier, which was the core mechanism of mutant catalytic efficiency improvement.

Enzymatic properties and degradation performance of mutants

To verify the independent contribution and synergistic effect of four mutation modules on enzyme performance, a systematic ablation experiment was conducted and demonstrated that all mutation modules could effectively enhance the substrate binding ability of the enzyme, reduce the activation energy barrier, and enhance the structural stability of the catalytic pocket. The four modules had significant synergistic effects. Among them, the introduction of Ser135Ala module alone could increase the relative enzyme activity to 245.32% and reduce the activation energy barrier by 1.88 kcal/mol. The relative enzyme activity of the double point mutant M3 increased to 290.45%,

Table 3. Core performance results of ablation experiments for wild-type and various mutants.

Enzyme type	Mutation module	Summary of Free Energy ΔG_bind (kcal/mol)	Catalytic pocket RMSF average value (nm)	Relative enzyme activity (%)
WT	None (wild type)	-27.80 ± 0.98	0.218 ± 0.012	100.00 ± 2.15
M1	Ser135Ala	-33.86 ± 0.87	0.195 ± 0.009	245.32 ± 3.26
M2	Val218Leu	-31.96 ± 0.91	0.202 ± 0.010	202.17 ± 2.89
M3	Gln180His/Thr245Ser	-34.97 ± 0.83	0.182 ± 0.008	290.45 ± 3.58
M4	Four-point full module combination	-44.60 ± 0.72	0.148 ± 0.006	551.24 ± 4.12

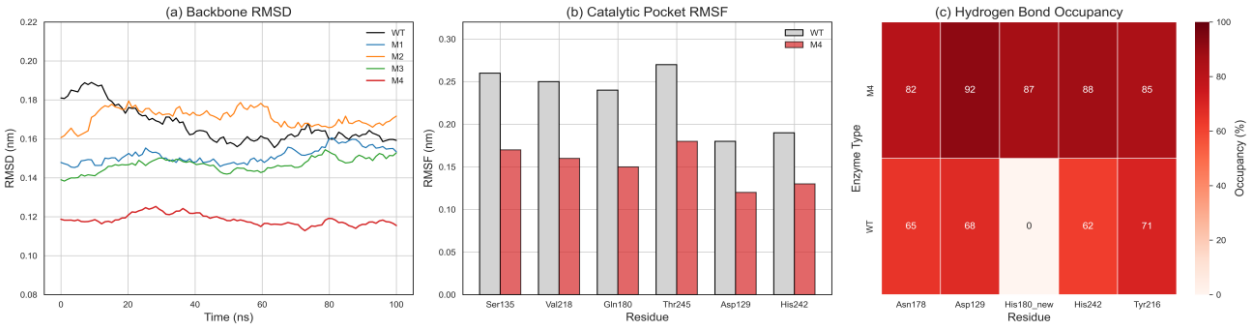

Figure 5. Molecular dynamics simulation structural stability analysis of wild-type and various mutants.

and the activation energy barrier decreased by 2.79 kcal/mol. The comprehensive improvement effect of the four site combination mutant M4 was the most significant with a total free energy reduction of 16.80 kcal/mol compared to the wild type, a reaction activation energy barrier reduction of 6.47 kcal/mol, an average root mean square fluctuation (RMSF) reduction of 32.1% in the catalytic pocket, and a relative enzyme activity 5.51 times that of the wild type, verifying the effectiveness of the multi module collaborative design strategy in this study (Table 3). Molecular dynamics simulation structural stability analysis showed that the main chain RMSD of the wild-type enzyme fluctuated continuously in the first 40 ns of simulation and finally stabilized at around 0.18 nm. The RMSD of all mutants reached equilibrium within 20 ns, and the RMSD of the optimal mutant M4 remained stable within 0.12 nm with significantly lower fluctuations than the wild type, indicating a significant enhancement in the overall structural stability of the enzyme after mutation (Figure 5a). The RMSF values of residues in the catalytic pocket region of wild-type enzymes were generally high, especially for ring residues such as Ser135, Val218, Thr245, *etc*. with RMSF values exceeding 0.25 nm. However, the RMSF values of catalytic pocket residues in mutant M4 decreased overall with an average decrease of 32%, indicating that the mutation significantly enhanced the structural rigidity of the catalytic pocket, reduced unnecessary conformational fluctuations, and was more conducive to stable substrate binding (Figure 5b). The core hydrogen bond occupancy rate between wild-type enzymes and substrates was generally below 70% with the hydrogen bond occupancy rate between the catalytic triad Asp129 and the substrate being only 68%. In mutant M4, the hydrogen bond occupancy rate between Asp129 and the substrate increased to 92%, and the

Table 4. Enzyme kinetic parameters of wild-type and various mutants.

Enzyme type	K_m (μg/mL)	V_{max} (μmol/min/mg)	k_{cat} (/s)	k_{cat}/K_m (mL/μg/s)	Relative catalytic efficiency
WT	12.64 ± 0.58	2.36 ± 0.11	3.12 ± 0.14	0.247 ± 0.012	1.00
M1	7.82 ± 0.35	3.58 ± 0.14	4.73 ± 0.18	0.605 ± 0.021	2.45
M2	8.57 ± 0.41	3.24 ± 0.13	4.28 ± 0.16	0.499 ± 0.018	2.02
M3	7.13 ± 0.32	3.87 ± 0.15	5.11 ± 0.19	0.717 ± 0.024	2.90
M4	4.81 ± 0.26	4.96 ± 0.18	6.55 ± 0.22	1.362 ± 0.031	5.51

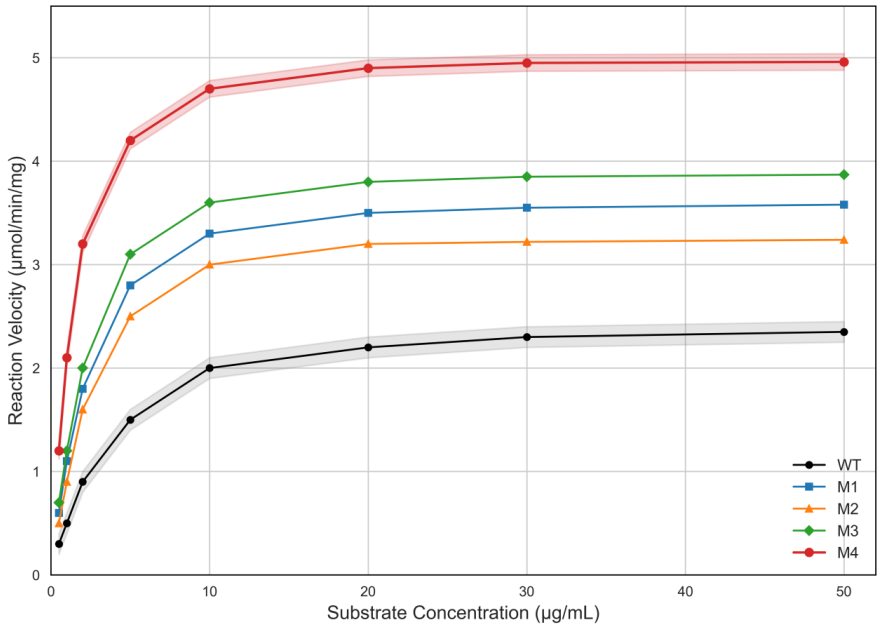

Figure 6. Michaelis-Menten kinetic fitting curves between wild-type and various mutants.

newly added His180 had a hydrogen bond occupancy rate of 87% with the substrate (Figure 5c). The overall stability of the hydrogen bond network was significantly enhanced, providing a stable microenvironment for substrate binding and catalytic reactions. To quantitatively evaluate the catalytic kinetic performance of each mutant, the initial rate of enzymatic reaction at different substrate concentrations measured was measured, and nonlinear fitting based on the Mie equation was performed to obtain the core enzyme kinetic parameters of the wild-type and each mutant. The results showed that the enzyme kinetics performance of all mutants was significantly better than that of the wild type with the four locus combination mutant M4 showing the most significant improvement effect. Compared with the wild type, the Miller constant K_m of M4 decreased from 12.64 μg/mL to 4.81 μg/mL, a decrease of 61.9%, indicating a significant increase in the affinity of the enzyme for DON substrate after mutation. The catalytic constant k_{cat} increased from 3.12/s to 6.55/s with a growth rate of 109.9%, indicating a significant enhancement in the enzyme's ability to catalyze substrate conversion. The final catalytic efficiency k_{cat}/K_m reached 1.362 mL/μg/s, which was 5.51 times that of the wild type, achieving dual optimization of substrate affinity and catalytic conversion ability, and meeting the expected design goals (Table 4). The Michaelis-Menten kinetic fitting curves of wild-type and various mutants were shown in Figure 6.

Table 5. Enzyme activity retention rates of wild-type and mutant M4 under different environmental conditions.

Environmental conditions	Group	Enzyme activity retention rate (%)	Environmental conditions	Group	Enzyme activity retention rate (%)
pH 4.0	WT	21.35 ± 1.24	30℃	WT	68.42 ± 1.56
	M4	75.68 ± 1.87		M4	82.35 ± 1.72
pH 4.5	WT	58.72 ± 1.56	35℃	WT	100.00 ± 2.15
	M4	96.48 ± 1.22		M4	92.47 ± 1.85
pH 5.5	WT	100.00 ± 2.15	40℃	WT	87.63 ± 1.68
	M4	100.00 ± 1.98		M4	98.72 ± 1.53
pH 7.0	WT	42.36 ± 1.38	45℃	WT	56.24 ± 1.42
	M4	95.13 ± 1.41		M4	100.00 ± 2.02
pH 8.0	WT	18.54 ± 1.02	50℃	WT	22.17 ± 1.15
	M4	68.25 ± 1.65		M4	76.38 ± 1.78
pH 9.0	WT	8.26 ± 0.58	60℃	WT	5.38 ± 0.32
	M4	32.47 ± 1.23		M4	38.62 ± 1.35

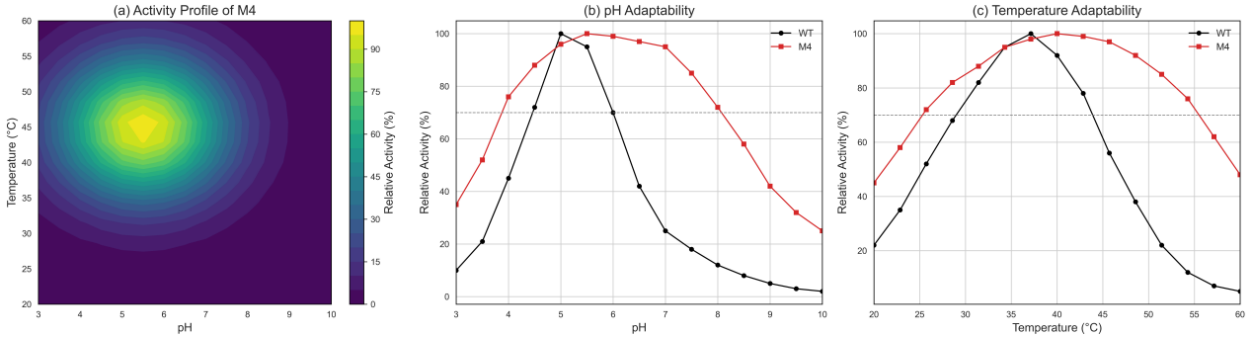

Figure 7. Environmental adaptability analysis of wild-type and optimal mutant M4.

To evaluate the impact of mutations on the environmental adaptability of enzymes, this study measured the enzyme activity retention rates of wild-type and optimal mutant M4 under different pH and temperature conditions. The results demonstrated that the optimal pH and temperature for the wild-type enzyme were 5.5 and 35℃, respectively. After deviating from the optimal conditions, the enzyme activity rapidly decreased. The optimal pH range of mutant M4 was 4.5 - 7.0, within which the enzyme activity retention rate remained above 95%. The optimal temperature of M4 increased from 35℃ to 45℃. Under acidic conditions of pH 4.0 and high temperature condition of 60℃, the enzyme activity retention rates of M4 reached 75.68% and 38.62%, respectively, which were more than three times higher than the wild type (Table 5). The results indicated that the mutation design in this study not only improved the catalytic efficiency of the enzyme, but also significantly enhanced its pH stability and thermal stability, increasing the environmental adaptability (Figure 7). To systematically evaluate the degradation ability of mutant M4 towards DON, this study conducted multiple experiments with different substrate concentrations, reaction temperatures, pH values, and reaction times. The results showed that mutant M4 maintained excellent DON degradation ability under a wide range of substrate concentrations, temperatures, and pH conditions. At a conventional substrate concentration of 10 μg/mL, the degradation rate was close to 90% after 30 minutes of reaction, and complete degradation could be achieved after 2 hours of reaction. When the substrate concentration reached 100 μg/mL, the degradation rate after 2 hours of reaction was

Table 6. Degradation efficiency of DON by mutant M4 under different reaction conditions.

Reaction time (h)	Substrate concentration (μ g/mL)	Temperature (℃)	PH value	DON degradation rate (%)
0.5	10	37	5.5	89.24 ± 2.15
1.0	10	37	5.5	97.61 ± 1.08
2.0	10	37	5.5	99.83 ± 0.12
2.0	50	37	5.5	95.37 ± 1.36
2.0	100	37	5.5	88.72 ± 1.89
2.0	10	45	5.5	99.76 ± 0.15
2.0	10	37	4.5	96.48 ± 1.22
2.0	10	37	7.0	95.13 ± 1.41
4.0	100	37	5.5	98.25 ± 0.87
6.0	200	37	5.5	92.46 ± 1.53

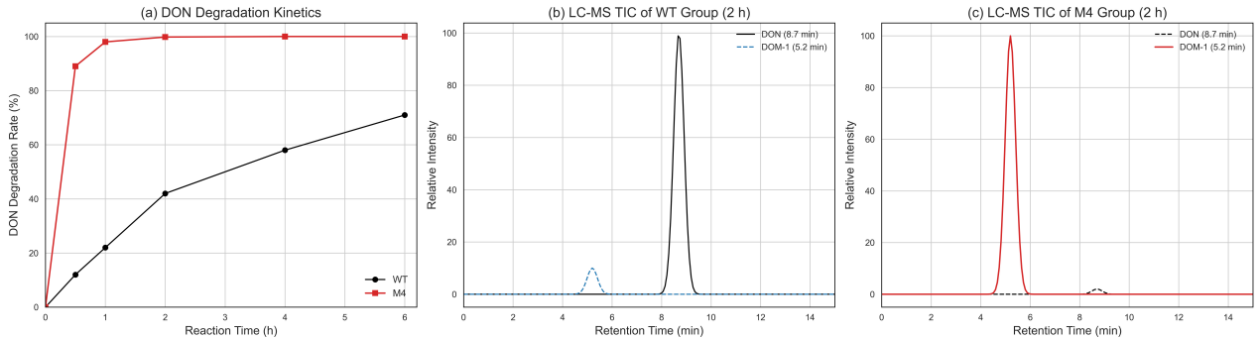

Figure 8. DON degradation kinetics and product analysis of wild-type and mutant M4.

still close to 90%, and the degradation rate after 4 hours of reaction could reach over 98%. Even in a high concentration substrate of 200 μg/mL, the degradation rate after 6 hours of reaction still exceeded 92%. Meanwhile, within the optimal temperature range of 45℃ and pH 4.5 - 7.0, M4 could maintain a degradation efficiency of over 95%, further verifying its excellent environmental adaptability and degradation performance (Table 6). The DON degradation kinetics and product analysis results showed that mutant M4 maintained the catalytic specificity of DON epoxide ring hydrolysis, generating only low toxicity DOM-1 products without any side reactions, and had good catalytic specificity and biosafety (Figure 8). To further validate the application performance of mutant M4 in actual grain processing scenarios, this study selected three main grain substrates including wheat, corn, and barley, which were naturally contaminated with DON. The degradation effect of M4 on DON was measured at different enzyme levels. The results showed that mutant M4 maintained excellent DON degradation efficiency in actual grain substrates. When the enzyme dosage was 5 U/g in wheat substrate, the degradation rate of DON at around 5 mg/kg reached 72.35%. When the enzyme dosage increased to 20 U/g, the degradation rate reached 92.17%, and the DON content decreased to 0.40 mg/kg after degradation, which was lower than 1.0 mg/kg, the DON limit requirement for grains and their products in the national food safety standards. In maize and barley substrates, the degradation rates under enzyme dosage of 20 U/g reached 88.64% and 85.72%, respectively, indicating that mutant M4 could adapt to the complex environment of different grain substrates and had good practical application potential (Table 7). The cyclic stability and

Table 7. DON degradation efficiency of mutant M4 in different grain matrices.

Cereal matrix	Initial DON content (mg/kg)	Enzyme dosage (U/g)	Reaction time (h)	DON degradation rate (%)	DON content after degradation (mg/kg)
Wheat	5.12 ± 0.21	5	2	72.35 ± 1.87	1.41 ± 0.08
	5.12 ± 0.21	10	2	85.64 ± 1.53	0.74 ± 0.05
	5.12 ± 0.21	20	2	92.17 ± 1.22	0.40 ± 0.03
Corn	4.87 ± 0.18	5	2	68.42 ± 1.76	1.54 ± 0.07
	4.87 ± 0.18	10	2	81.25 ± 1.48	0.91 ± 0.04
	4.87 ± 0.18	20	2	88.64 ± 1.35	0.55 ± 0.04
Barley	5.34 ± 0.23	5	2	65.18 ± 1.69	1.86 ± 0.09
	5.34 ± 0.23	10	2	78.36 ± 1.55	1.15 ± 0.06
	5.34 ± 0.23	20	2	85.72 ± 1.42	0.76 ± 0.05

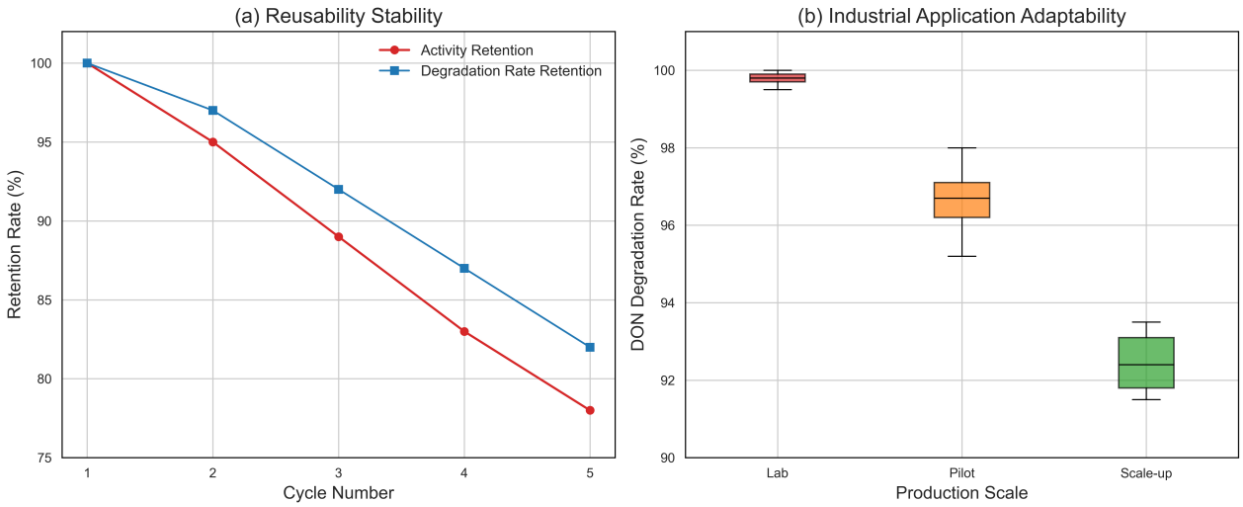

Figure 9. Analysis of cycle stability and industrial applicability of mutant M4.

industrial applicability analysis demonstrated that, after 5 cycles of use, the enzyme activity retention rate of M4 could still reach 78.26%, and the degradation rate of DON remained above 80%, indicating that the mutant had good operational stability and could meet the application requirements of industrial continuous degradation. The degradation rate of DON by M4 remained stable in laboratory small-scale, simulated pilot, and large-scale production systems with average degradation rates of 99.83%, 96.72%, and 92.45%, respectively, without significant performance degradation (Figure 9). The results indicated that the mutant had good industrial scaling adaptability and the potential for large-scale industrial applications.

Summary and implications

This study successfully constructed a multi-scale computational design combined with site-directed mutagenesis strategy for the targeted modification of *Fusarium oxysporum* DON detoxifying enzyme. Through the reconstruction of catalytic pocket microenvironment, optimization of hydrogen bond network, and stabilization of transition state, the improvement of enzyme catalytic efficiency, substrate affinity, and environmental stability were achieved simultaneously. The optimal four-site combination mutant M4 showed 5.51-fold higher catalytic efficiency than the wild type, significantly expanded pH and temperature adaptation ranges, and excellent degradation performance in both liquid phase systems and

actual grain substrates. The mutant also maintained good catalytic specificity and cyclic stability, demonstrating great potential for industrial application. This study provided a scalable technical path for the efficient modification of fungal toxin detoxifying enzymes and other industrial enzymes and core materials and technical support for the green biological detoxification of grain fungal toxins. However, the stability of this mutant in high concentration organic systems and the cost control of large-scale fermentation expression still need further optimization. Future research should combine protein surface charge engineering and immobilization technology to further enhance the industrial application performance of the enzyme. Meanwhile, a multi-enzyme collaborative degradation system may be constructed to achieve synchronous and efficient detoxification of multiple fungal toxins.

References

1. Adegoke TV, Lu S, Adegoke OG, Wang Y, Zhang L, Li J, *et al*. 2025. Optimizing single and cascade microbial enzyme systems through site-directed mutagenesis for enhancing mycotoxin detoxification. Biotechnol Adv. 47:108751.
2. Enguita FJ, Leitão AL. 2025. Cross-Kingdom enzymatic strategies for deoxynivalenol detoxification: Computational analysis of structural mechanisms and evolutionary adaptations. Microorganisms. 13(10):2384.
3. Pedroni L, Doherty DZ, Dall'Asta C, Battilani P, Sulyok M, Krska R, *et al*. 2024. Computational methods meet *in vitro* techniques: A case study on fusaric acid and its possible detoxification through cytochrome P450 enzymes. Ecotoxicol Environ Saf. 273:116167.
4. Luo K, Guo J, He D, Zhang Y, Wang X, Li Z, *et al*. 2023. Deoxynivalenol accumulation and detoxification in cereals and its potential role in wheat–*Fusarium graminearum* interactions. Abiotech. 4(2):155-171.
5. Sun Y, Li S, Liu S, Wang H, Zhang Y, Zhao J, *et al*. 2026. Advances in microbial and enzymatic degradation of deoxynivalenol (DON). J Agric Food Chem. 74:3215-3232.
6. Della Gala V. 2025. Enzymatic strategies for xenobiotic and mycotoxin detoxification. J Biotechnol Res. 12:456-472.
7. Zhou Y, Qiu FJ, Li JB, Wang L, Zhang H, Liu Y, *et al*. 2025. Characterization of ZPH13 phosphotransferase from *Bacillus subtilis* in zearalenone transformation. Protein Expr Purif. 223:106783.
8. Wang Y, Yang L, Xu J, Chen L, Zhang H, Li Y, *et al*. 2023. Applications of synthetic microbial consortia in biological control of mycotoxins and fungi. Curr Opin Food Sci. 53:101074.
9. Iñiguez-Luna MI, Cadena-Zamudio JD, Ramírez-Mosqueda MA, García-Pérez JS, Rodríguez-Herrera R, Aguilar CN. 2025. Molecular docking as a key driver of biocontrol for agri-food security. BioTech. 14(4):80.
10. Yang Z, Zhou N, Jiang X, Wang Y, Li S, Zhang L, *et al*. 2023. Loop evolutionary patterns shape catalytic efficiency of TRI101/201 for trichothecenes: Insights into protein–substrate interactions. J Chem Inf Model. 63(20):6316-6331.
11. Dumbai Joe A, Liu R, Luo X, Wang Y, Zhang H, Li J, *et al*. 2025. Comprehensive analysis of the mechanisms conferring resistance to phenamacril in the *Fusarium* species. Front Cell Infect Microbiol. 15:1536532.
12. Varadharajan V, Rajendran R, Muthuramalingam P, Ramesh M, Pandian SK. 2025. Multi-omics approaches against abiotic and biotic stress — A review. Plants. 14(6):865.
13. Chtioui W, Balmas V, Delogu G, Migheli Q, Scherm B. 2022. Bioprospecting phenols as inhibitors of trichothecene-producing *Fusarium*: Sustainable approaches to the management of wheat pathogens. Toxins. 14(2):72.
14. Tundo S, Mandalà G, Sella L, Favaron F, D'Ovidio R. 2022. Xylanase inhibitors: Defense players in plant immunity with implications in agro-industrial processing. Int J Mol Sci. 23(23):14994.
15. Mateo F, Mateo EM, Tarazona A, García-Díaz MT, Jiménez M. 2025. New strategies and artificial intelligence methods for the mitigation of toxigenic fungi and mycotoxins in foods. Toxins. 17(5):231.
16. Schueller A, Studt-Reinhold L, Strauss J. 2022. How to completely squeeze a fungus — advanced genome mining tools for novel bioactive substances. Pharmaceutics. 14(9):1837.
17. Narula K, Ghosh S, Khan IN, Singh R, Kumar A, Pandey AK, *et al*. 2026. Cross-Kingdom global proteomics reveals specific modulation of disease signaling in multi-host fungal pathogen infection in chickpea and worm. J Proteome Res. 25:1123-1135.
18. Younas A, Rashid M, Riaz N, Hussain MA, Anjum MA. 2023. Emerging techniques to develop biotic stress resistance in fruits and vegetables. In: Sustainable agriculture in the era of the OMICs revolution. Cham: Springer International Publishing. 2023:269-296.
19. He WJ, Yang P, Huang T, Wang X, Li J, Zhang Y, *et al*. 2024. Detoxifying bacterial genes for deoxynivalenol epimerization confer durable resistance to *Fusarium* head blight in wheat. Plant Biotechnol J. 22(9):2395-2409.
20. Yang H, Yan R, Li Y, Wang X, Zhang H, Li J, *et al*. 2022. Structure–function analysis of a quinone-dependent dehydrogenase capable of deoxynivalenol detoxification. J Agric Food Chem. 70(22):6764-6774.
21. Li D, Liang G, Mu P, Wang Y, Zhang H, Li J, *et al*. 2023. Improvement of catalytic activity of sorbose dehydrogenase for deoxynivalenol degradation by rational design. Food Chem. 423:136274.
22. Hu Y, Li H, Min J, Wang X, Zhang H, Li J, *et al*. 2022. Crystal structure and biochemical analysis of the specialized deoxynivalenol–detoxifying glyoxalase SPG from *Gossypium hirsutum*. Int J Biol Macromol. 200:388-396.

23. Yang J, Liang K, Ke H, Wang X, Zhang H, Li J, *et al*. 2024. Enzymatic degradation of deoxynivalenol with the engineered detoxification enzyme Fhb7. JACS Au. 4(2):619-634.
24. Huang J, Zhang X, Zhang H, Wang X, Li J, Zhang Y, *et al*. 2025. Addressing clinical limitations of glutaminase inhibitors: Novel strategies for osimertinib-resistant lung cancer by exploiting glutamine metabolic dependency. Adv Sci. 12(6):2411479.
25. Paclikova P, Harnos J. 2024. Efficient cloning of linear DNA inserts (ECOLI) into plasmids using site-directed mutagenesis. Sci Rep. 14(1):21591.
26. Luan J, Song C, Liu Y, Wang X, Zhang H, Li J, *et al*. 2024. Seamless site-directed mutagenesis in complex cloned DNA sequences using the RedEx method. Nat Protoc. 19(11):3360-3388.
27. Wang G, Wang M, Liu L, Wang X, Zhang H, Li J, *et al*. 2022. Improvement of the catalytic performance of glycerol kinase from *Bacillus subtilis* by chromosomal site-directed mutagenesis. Biotechnol Lett. 44(9):1051-1061.
28. Fengmin L, Heng Z, Xiangjun Z, Wang X, Zhang H, Li J, *et al*. 2023. Site-directed mutagenesis improves the practical application of L-glutamic acid decarboxylase in *Escherichia coli*. Eng Life Sci. 23(4):e2200064.
29. Fu B, Chen M, Bao X, Wang X, Zhang H, Li J, *et al*. 2024. Site-directed mutagenesis of bifunctional riboflavin kinase/FMN adenylyltransferase *via* CRISPR/Cas9 to enhance riboflavin production. Synth Syst Biotechnol. 9(3):503-512.
30. Xing H, Wang P, Yan X, Wang X, Zhang H, Li J, *et al*. 2023. Thermostability enhancement of *Escherichia coli* phytase by error-prone polymerase chain reaction (epPCR) and site-directed mutagenesis. Front Bioeng Biotechnol. 11:1167530.